Aust. J. Phys., 1983, **36**, 197–219

Flow Distribution in Parallel Connected Manifolds for Evacuated Tubular Solar Collectors

R. C. McPhedran, D. J. M. Mackey, D. R. McKenzie and R. E. Collins

School of Physics, University of Sydney, Sydney, N.S.W. 2006.

Abstract

A model is presented for predicting the flow distribution in solar collector manifolds in which risers are connected in parallel between headers. Both frictional and Bernoulli effects are considered. The distributions resulting from flow in the manifold in which header streams are parallel and opposed are calculated and compared with experiment. Parallel flow gives a more uniform distribution. The outlet header is found to be more critical in balancing the flow distribution than the inlet header. Conditions under which thermosiphon effects are important and flow reversal in risers may occur are discussed with reference to experiment.

1. Introduction

Consider the flow of a liquid in a system such as that of Fig. 1. Two tubes, respectively called the inlet and outlet headers, are connected by a large number of tubes called risers all connected in parallel. Flow of liquid through the system is achieved by pumping. We wish to calculate the distribution of the total flow among the various riser tubes, and to compare it with experimental distributions.

In an important practical occurrence of this problem, the risers are placed inside evacuated tubular solar collectors, and the liquid in the risers is heated by heat conducted through the riser walls. The temperature change of the fluid between its entry into and its exit from a particular riser is governed by the flow rate in the riser. A uniform partition of flow is desirable as it ensures that the fluid temperature change along each riser is the same. This in turn enables equally efficient operation of all the tubes making up the collector.

The model we develop will apply to situations where the flow distribution is nearly uniform and where the temperature changes of the fluid along risers are sufficiently small to make buoyancy effects negligible. (This is the isothermal flow assumption; its use will restrict our model to forced-flow collector systems.)

Previous analyses of flow distributions in solar collector manifolds have been of two types. Jones and Lior (1978) used a discrete model, restricted to a fairly small number N of risers ($N \leqslant 30$). Each riser is represented by an element in a vector of flow rates, and a system of nonlinear algebraic equations is solved to find this vector. As well as being restricted to fairly small systems, such a numerical model does not give great insight into the way the various parameters of the manifold system influence the flow pattern in the risers.

0004-9506/83/020197$02.00

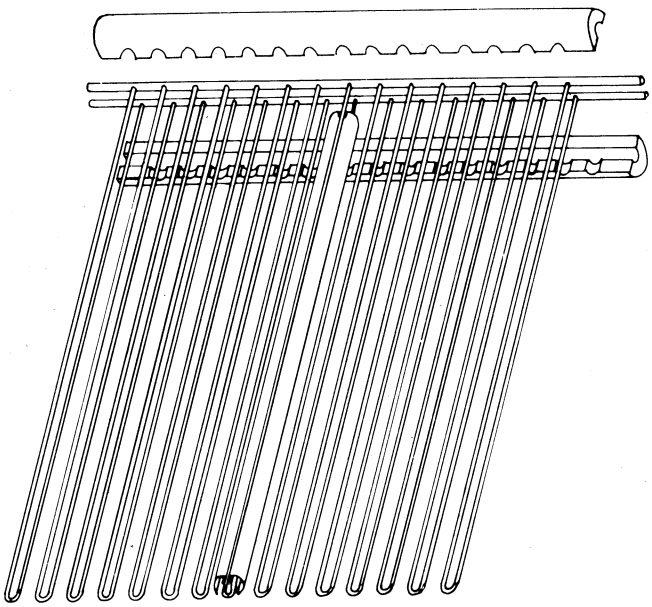

Fig. 1. A Sydney University evacuated tubular collector module, with 15 risers connecting the inlet and outlet headers. The metal fin shown on the eighth riser (and actually present on all 15) provides good thermal contact between the collector tubes and risers. The two headers are provided with thermal insulation, as shown.

Dunkle and Davey (1970) developed a continuous model for flow distribution. In their model, the number of risers is supposed to be sufficiently large so that pressure and flow rates vary smoothly along the manifold, and are accurately represented by continuous functions. Dunkle and Davey set up a differential equation for the flow rate in the output header, and were able to obtain a simple expression for this in terms of hyperbolic functions.

Dunkle and Davey's principal conclusion was that the key factor governing the uniformity of the riser flow distribution was a number β relating the pressure drop in the headers to the pressure drop in the risers. When β is large, flow is concentrated in the risers closest to the manifold inlet and outlet (the end risers). When β is small, flow is uniformly distributed among the risers.

The model described here is more general than that by Dunkle and Davey, and incorporates a number of features permitting a more accurate representation of flow conditions. Firstly, we allow for Bernoulli effects on the flow distribution. These effects are important in that they break the symmetry between the inlet and outlet headers present in the model by Dunkle and Davey, making the outlet header the more critical. Secondly, Dunkle and Davey assumed flow in the headers to be turbulent at all flow rates, as a result of form turbulence induced by projections of the risers into the headers. In a carefully constructed manifold this will not be the case, and so we model the header flow according to its Reynolds number. Thirdly, following Dunkle and Davey, we assume laminar flow in the risers, the pressure drop along them varying linearly with flow rate. Here we add a quadratic term to the linear one, in order to allow for pressure drop on entry to the riser, on traversal of the riser bend (see Fig. 1) and on exit from the riser.

In our discussion of manifold flow, we will be guided by the work of Bajura (1971) and Bajura and Jones (1976). These authors have carefully considered flow in the neighbourhood of branch points, such as those where risers meet headers. They advocated the use of momentum conservation rather than energy conservation in modelling flow near such points, on the basis that it is very difficult to allow properly for localized heating effects around the junction as mechanical energy is lost through viscous dissipation.

In order to show the physical origin of the various terms in the generalized flow equations of Bajura and Jones (1976), we give a brief derivation of them in Section 4. We also discuss how values may be chosen for the various flow parameters in the case of a particular manifold which has been used in solar collector arrays. We write the flow equations in a form amenable to numerical solution using a standard algorithm for the solution of two-point boundary value problems in Section 5.

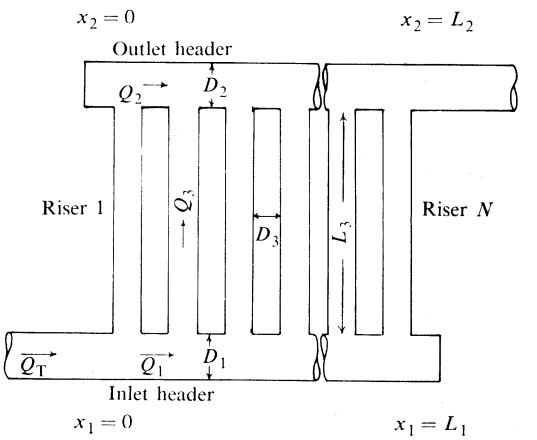

Fig. 2. Simplified schematic diagram of a manifold, showing the flow rates (Q_T, Q_1, Q_2 and Q_3), the lengths and diameters (L_1, D_1, L_2, D_2, L_3 and D_3), and the coordinates x_1 and x_2 for the inlet and outlet headers.

Having thus developed a numerical method of calculating flow distributions, we study in Section 7 the behaviour of these distributions in the chosen manifold. We show that the parallel flow situation shown in Fig. 2 gives (in general) better flow uniformity than the reverse flow situation (in which the flow in the outlet header has the opposite direction to that in the inlet header). We also show that the ratio of riser to header diameters is the crucial parameter governing flow uniformity. We discuss the physical reasons for these and other facets of manifold behaviour. We describe the method by which the flow distribution in the manifold was measured, and compare the results of these measurements with the theoretical predictions.

2. Flow at a Dividing Branch Point

Consider the situation shown in Fig. 3. We take a control volume of length Δx_1, enclosing the junction between a typical riser and the inlet header. If L_1 denotes the length of the inlet header, and N_1 the number of risers intersecting it, we choose

$$\Delta x_1 = L_1/N_1 . \tag{1}$$

The downstream and upstream surfaces A_{11} and A_{12} have a common area A_1, while the riser section A_{31} has area A_3. We use v_1 to denote fluid speed at a typical

point in A_{11}, and $\bar{v}_1$ to denote the value of v_1 averaged over A_{11}. We similarly define v_2 and $\bar{v}_2$ for A_{12}. The mean riser speed is called $\bar{v}_3$. Following the terminology of Bajura and Jones (1976), we introduce velocity components v_x and v_y for the fluid entering the riser through A_{31}, allowing for the fact that the fluid will not have changed its direction of flow by 90° when it crosses this surface.

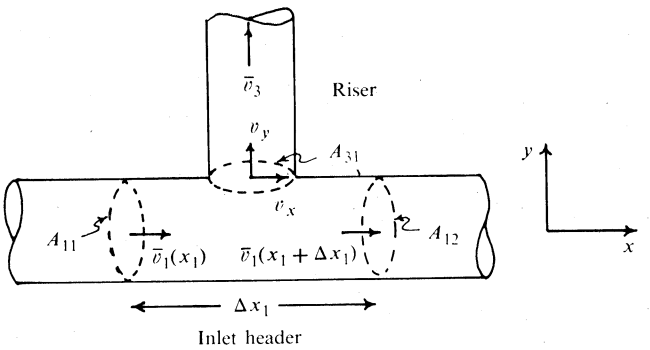

Fig. 3. Typical riser junction with the inlet header. The areas A_{11}, A_{12} and A_{31}, together with the wall of the inlet header, define a control volume within which the conservation of flow momentum is applied.

Let us write down the momentum equation for the control volume of Fig. 3, considering only the x components of momentum. We must allow for losses of momentum through drag forces associated with viscosity and with the roughness of the side walls. Using P to denote pressure and T_W to denote the wall shear stress associated with the above drag forces, we write

$$\int_{A_{11}} P\,\mathrm{d}A - \int_{A_{12}} P\,\mathrm{d}A - \int_{SW} T_W\,\mathrm{d}A$$
$$= \int_{A_{12}} \rho v_2^2\,\mathrm{d}A - \int_{A_{11}} \rho v_1^2\,\mathrm{d}A + \int_{A_{31}} \rho v_x v_y\,\mathrm{d}A\,. \tag{2}$$

In equation (2), SW denotes that part of the header side wall lying within the control volume, while the form of the third term on the RHS reflects the fact that we are interested in the x component of momentum, where v_y controls the mass of fluid passing through A_{31} in unit time and ρ denotes fluid density.

We now rewrite equation (2) in terms of average velocities and pressures. To do this, we introduce a correction factor for the axial flow of momentum

$$\beta_1 = \frac{1}{A_1 \bar{v}_1^2} \int_{A_{11}} v_1^2\,\mathrm{d}A_1\,. \tag{3}$$

At this stage we will allow for the possibility that β_1 may depend on x_1. We also introduce a correction factor for the axial momentum of fluid entering the riser

$$\gamma_1 = \frac{1}{\bar{v}_1 \bar{v}_3 A_3} \int_{A_{31}} v_x v_y\,\mathrm{d}A_3\,. \tag{4}$$

The third integral on the LHS of equation (2) is related to the pressure drop along the length Δx_1 due to viscous and wall effects. This pressure drop is related to the

Moody friction factor f_1 for the inlet header and to the square of the mean speed $\bar{v}_1^2$ (Kenyon 1960):

$$\int_{SW} T_W \, dA = f_1 \rho \bar{v}_1^2 \pi_1 L_1 / 8N_1 , \tag{5}$$

where π_1 denotes the circumference of the header.

The Moody friction factor f_1 depends on the Reynolds number R_1 for flow in the header, as well as the relative roughness of the header walls. A plot of f_1 against R_1 for various values of relative roughness is termed a Moody diagram (see e.g. Hansen 1967). Assuming a value of 0·025 for the ratio of pipe roughness to diameter, we adopt for the numerical examples given below the following variation of f_1 with R_1:

$$f_1 = 64/R_1 \qquad \text{for } R_1 < 2000, \tag{6a}$$

$$= 0{\cdot}009 + (1{\cdot}150 \times 10^{-5}) R_1 \qquad \text{for } 2000 < R_1 < 4000, \tag{6b}$$

$$= 0{\cdot}055 \qquad \text{for } R_1 > 4000. \tag{6c}$$

The expression (6a) corresponds to laminar flow, (6c) to fully developed roughness-dominated turbulent flow, while (6b) provides for a linear increase of f_1 from one limiting value to another over the critical zone. The Reynolds number R_1 is connected to the fluid viscosity μ and its mean velocity $\bar{v}_1$ by

$$R_1 = \rho \bar{v}_1 D_1 / \mu , \tag{7}$$

where D_1 is the diameter of the inlet header.

Returning to equation (2), we rewrite it in terms of mean pressures and fluid speeds, while neglecting all terms of order two or higher in Δx_1:

$$\frac{1}{\rho} \frac{d\bar{P}_1}{dx_1} + \left(\frac{f_1 \pi_1}{8A_1} + \frac{d\beta_1}{dx_1} \right) \bar{v}_1^2 + \theta_1 \bar{v}_1 \frac{d\bar{v}_1}{dx_1} = 0. \tag{8}$$

In equation (8) we have

$$\theta_1 = 2\beta_1 - \gamma_1 . \tag{9}$$

To the same order of accuracy as in (8), we express the conservation of flow at the junction as

$$\bar{v}_3 A_3 = -A_1 \frac{d\bar{v}_1}{dx_1} \frac{L_1}{N_1} . \tag{10}$$

It will be noticed in (8) that it is the changes in the axial momentum correction factor β_1 which are more important than the actual value of β_1. If there is an asymmetric flow pattern entering the inlet header, then β_1 may well decrease until the equilibrium flow pattern is attained. It is then possible to have $d\beta_1/dx_1$ negative for small values of x_1, so that the frictional loss term $f_1 \pi_1 / 8A_1$ can be reduced or even reversed in sign. Bajura and Jones (1976) used the term $d\beta_1/dx_1$ to account for the reversal of flow which sometimes occurs in poorly designed manifolds; we comment further on this in Section 9. (This reversal of flow refers to the case when $\bar{v}_3$ in Fig. 3

is in fact negative, so that riser fluid enters the inlet header.) In our numerical examples, we will assume the velocity profile across each header to be independent of x, leading to a value of zero for each $d\beta/dx$.

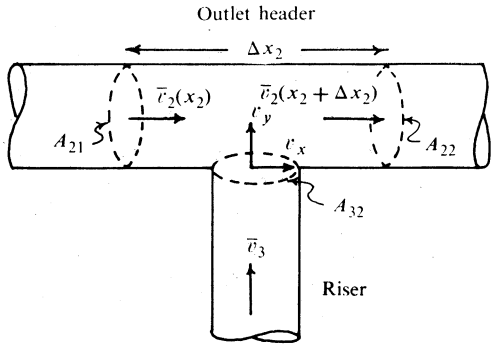

Fig. 4. Typical riser junction with the outlet header. The areas A_{21}, A_{22} and A_{32}, together with the wall of the outlet header, define a control volume within which the conservation of flow momentum is applied.

3. Flow at a Combining Branch Point

Let us consider the conservation of axial momentum for the control volume shown in Fig. 4, where we depict the situation for a parallel flow manifold. (We will not go through the calculations for a reverse flow manifold here, but give only the final differential equations from which the flow patterns may be deduced.) The equation analogous to (2) is then

$$\int_{A_{21}} P\,dA - \int_{A_{22}} P\,dA - \int_{SW} T_W\,dA = \int_{A_{22}} \rho v_2^2\,dA - \int_{A_{21}} \rho v_1^2\,dA - \int_{A_{32}} \rho v_x v_y\,dA. \tag{11}$$

We express velocity components in equation (11) in terms of mean fluid flow rates, introducing the analogue of θ_1 for the outlet header

$$\theta_2 = 2\beta_2 - \gamma_2. \tag{12}$$

We also replace integrated pressures by the cross sectional area times the appropriate mean pressure, and use the analogue of equation (5) to evaluate the third integral on the LHS of (11). Retaining only zeroth and first-order terms in $\Delta x_2 = L_2/N_2$, the equation expressing conservation of flow at the junction becomes

$$\bar{v}_3 A_3 = A_2 \frac{d\bar{v}_2}{dx_2}\frac{L_2}{N_2}, \tag{13}$$

while (11) yields an equation of the same form as (8):

$$\frac{1}{\rho}\frac{d\bar{P}_2}{dx_2} + \left(\frac{f_2\pi_2}{8A_2} + \frac{d\beta_2}{dx_2}\right)\bar{v}_2^2 + \theta_2 \bar{v}_2 \frac{d\bar{v}_2}{dx_2} = 0. \tag{14}$$

At this stage in the analysis, there are four unknown functions, namely the pressures $\bar{P}_1$ and $\bar{P}_2$, together with the flow speeds $\bar{v}_1$ and $\bar{v}_2$. However, the last two quantities are related by a continuity equation ensuring that flow leaving one header enters the other:

$$\bar{v}_2 = (\bar{v}_{1,0} - \bar{v}_1) A_1 / A_2 , \tag{15}$$

where $\bar{v}_{1,0}$ is the average speed at the start of the inlet header.

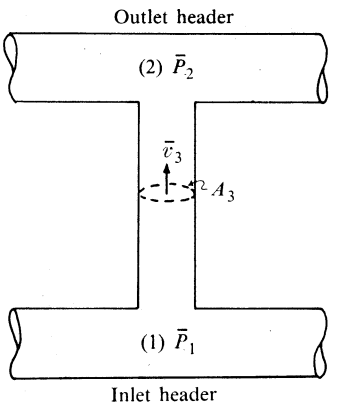

Fig. 5. Pressure drop across a riser. The Bernoulli equation is used to link the pressures $\bar{P}_1$ and $\bar{P}_2$ at points (1) and (2). It is assumed that transverse flow starts at point (1), and that at (2) it still has the speed $\bar{v}_3$. Corrections are made for the turning of the flow around points (1) and (2).

4. Pressure Flow Equations

Let us now consider the pressure drop across a riser. We write a Bernoulli equation linking points (1) and (2) in Fig. 5, where it is assumed that transverse flow starts at (1), and that at (2) it still has the speed $\bar{v}_3$. We introduce a coefficient c_{TD} to account for the pressure loss involved in the turning of the flow around point (1). (Here we say that the pressure at a point just inside the riser is not $\bar{P}_1$, but $\bar{P}_1 - \frac{1}{2}\rho \bar{v}_3^2 c_{TD}$ due to this turning pressure loss.) We also introduce a coefficient c_{TC} as a correction for turning loss around (2). (Here we say that the pressure at a point just inside the riser on the outlet side is not $\bar{P}_2$, but $\bar{P}_2 + \frac{1}{2}\rho \bar{v}_3^2 c_{TC}$.) We denote the riser length and diameter by L_3 and D_3 respectively, while the friction factor in the riser is f_3. Also, an additional coefficient K_3 is introduced to account for any pressure losses within the riser not caused by friction. [Note that in Fig. 1 the risers have a 180° bend; $K_3 = 2{\cdot}20$ is an estimate (Swanson 1970) of the loss coefficient appropriate to such a bend.] The Bernoulli equation linking points (1) and (2) is then

$$\bar{P}_1/\rho = \bar{P}_2/\rho + \tfrac{1}{2}\bar{v}_3^2 + \tfrac{1}{2}\bar{v}_3^2 (c_{TD} + K_3 + f_3 L_3/D_3 + c_{TC}) . \tag{16}$$

Let us introduce a coefficient H_3 to account for all flow-dependent terms on the RHS of equation (16):

$$H_3 = 1 + c_{TD} + c_{TC} + K_3 + f_3 L_3/D_3 . \tag{17}$$

Let us also call $\Delta\bar{P}_{12}$ the differential pressure between the headers:

$$\Delta\bar{P}_{12}/\rho = (\bar{P}_1 - \bar{P}_2)/\rho = \tfrac{1}{2} H_3 \bar{v}_3^2 . \tag{18}$$

We can use equation (10) to eliminate $\bar{v}_3$ from (18):

$$\Delta\bar{P}_{12}/\rho = \tfrac{1}{2} H_3 \left(\frac{A_1 L_1}{A_3 N_1} \frac{d\bar{v}_1}{dx_1} \right)^2 . \tag{19}$$

We can solve equation (19) for $d\bar{v}_1/dx_1$, remembering that $\bar{v}_1$ must decrease as x_1 increases (flow being lost from the inlet to the outlet header):

$$\frac{d\bar{v}_1}{dx_1} = -\frac{N_1 A_3}{L_1 A_1}(2/\rho H_3)^{\frac{1}{2}}(\Delta\bar{P}_{12})^{\frac{1}{2}}, \tag{20}$$

where both H_3 and $\Delta\bar{P}_{12}$ must be positive functions. We can combine equations (8) and (14) to obtain for $\Delta\bar{P}_{12}$

$$\frac{1}{\rho}\frac{d(\Delta\bar{P}_{12})}{dx} = -\left\{\left(\frac{f_1 \pi_1 L_1}{8A_1} + \frac{d\beta_1}{dx}\right)\bar{v}_1^2 + \theta_1 \bar{v}_1 \frac{d\bar{v}_1}{dx}\right\}$$
$$+\left\{\left(\frac{f_2 \pi_2 L_2}{8A_2} + \frac{d\beta_2}{dx}\right)\bar{v}_2^2 + \theta_2 \bar{v}_2 \frac{d\bar{v}_2}{dx}\right\}, \tag{21}$$

in which we use the non-dimensional length variable

$$x = x_1/L_1 = x_2/L_2. \tag{22}$$

Let us now introduce the non-dimensional variables for flow speed and pressure difference

$$v = \bar{v}_1/\bar{v}_{1,0}, \tag{23}$$

$$\Delta P = \Delta\bar{P}_{12}/\rho\bar{v}_{1,0}^2. \tag{24}$$

From equation (15), we see that

$$\bar{v}_2/\bar{v}_{1,0} = (1-v)A_1/A_2. \tag{25}$$

From (22)–(24), equation (20) becomes

$$\frac{dv}{dx} = -\frac{N_1 A_3}{A_1}(2/H_3)^{\frac{1}{2}}(\Delta P)^{\frac{1}{2}}, \tag{26}$$

while equation (21) becomes

$$\frac{d(\Delta P)}{dx} = -\left(\frac{f_1 \pi_1 L_1}{8A_1} + \frac{d\beta_1}{dx}\right)v^2 + \left(\frac{f_2 \pi_2 L_2}{8A_2} + \frac{d\beta_2}{dx}\right)(1-v)^2\frac{A_1^2}{A_2^2}$$
$$-\theta_1 v\frac{dv}{dx} - \theta_2\left(\frac{A_1}{A_2}\right)^2(1-v)\frac{dv}{dx}. \tag{27}$$

Bajura and Jones (1976) wrote the pressure flow equations (26) and (27) in the generalized form

$$\frac{dv}{dx} = -Z(\Delta P)^{\frac{1}{2}}, \tag{28}$$

$$\frac{d(\Delta P)}{dx} = -A_1 v^2 + A_2(1-v)^2 - B_1 v\frac{dv}{dx} - B_2(1-v)\frac{dv}{dx}. \tag{29}$$

Let us define

$$A_r = N_1 A_3/A_1, \tag{30}$$

the area ratio of the total cross sectional area of the risers to that of the inlet header. For the parallel flow manifolds considered thus far we have

$$Z = A_r(2/H_3)^{\frac{1}{2}}, \tag{31}$$

$$A_1 = \frac{f_1 L_1}{2D_1} + \frac{d\beta_1}{dx}, \qquad A_2 = \left(\frac{f_2 L_2}{2D_2} + \frac{d\beta_2}{dx}\right)\left(\frac{D_1}{D_2}\right)^4, \tag{32a, b}$$

$$B_1 = \theta_1, \qquad B_2 = \theta_2(D_1/D_2)^4. \tag{32c, d}$$

In equations (32), we have taken the case of headers of circular cross section, replacing A_1 by $\frac{1}{4}\pi D_1^2$ and A_2 by $\frac{1}{4}\pi D_2^2$.

In the case of reverse flow manifolds, the flow speed in the outlet header is not given by equation (25), but rather by

$$\bar{v}_2/\bar{v}_{1,0} = vA_1/A_2. \tag{33}$$

Equations (28)–(31) are unaltered, while (32) become

$$A_1 = \frac{f_1 L_1}{2D_1} + \frac{f_2 L_2}{2D_2}\left(\frac{D_1}{D_2}\right)^4 + \frac{d\beta_1}{dx} - \left(\frac{D_1}{D_2}\right)^4 \frac{d\beta_2}{dx}, \qquad A_2 = 0, \tag{34a, b}$$

$$B_1 = \theta_1 - (D_1/D_2)^4\theta_2, \qquad B_2 = 0. \tag{34c, d}$$

The pressure flow equations (28) and (29) have to be solved subject to the boundary conditions

$$v(0) = 1, \qquad v(1) = 0. \tag{35}$$

Table 1. Dimensions of the solar collector manifold

The material is hard drawn copper; the header is silver soldered to the riser joints; the heat transfer medium is water

Description	Dimension
Riser pipe internal diameter	4·4 mm
Header pipes internal diameter	17·1 mm
Spacing between risers	60 mm
Total length of risers	2·9 m
Projection of riser ends into header	$\leqslant$ 1 mm

5. Pressure Flow Equations for a Collector Manifold

Let us now consider the form taken by the pressure flow equations when the various parameters are given the values appropriate to the manifold of Fig. 1, with dimensions as in Table 1. Firstly, the length of each header is the same and is dependent on the common number of risers intersecting both inlet and outlet headers:

$$N_1 = N_2 = N, \tag{36}$$

$$L_1 = L_2 = L = \tfrac{1}{15}N. \tag{37}$$

Secondly, in order to keep the temperature gradient across each riser uniform when the flow pattern is uniform, the total volume flow rate of liquid Q_T is scaled according to the number of risers, being based on a typical figure in practice of 1 L min^{-1} for $N = 15$,

$$Q_T = \tfrac{1}{4}\pi D_1^2 \bar{v}_{1,0} = \tfrac{1}{15}N \times 1{\cdot}6667 \times 10^{-5}\ \mathrm{m^3\,s^{-1}}. \tag{38}$$

Thirdly, we assume the velocity profiles across each header to be stable within the manifold,

$$\mathrm{d}\beta_1/\mathrm{d}x = \mathrm{d}\beta_2/\mathrm{d}x = 0, \tag{39}$$

the constant values of β_1 and β_2 being close to unity,

$$\beta_1 \approx \beta_2 \approx 1. \tag{40}$$

From the work of Bajura and Jones (1976), the approximations (39) and (40) are accurate for systems in which sharp bends do not occur in the header pipes leading into and out of the manifold. It would be very difficult to calculate the coefficients γ_1 and γ_2 as a function of junction geometry and flow rates, so we use estimates for them based on previous experimental studies. From data by Bajura (1971), we estimate γ_1 to be close to unity, and largely independent of the ratio of riser to header flow:

$$\theta_1 = 2\beta_1 - \gamma_1 \approx 1. \tag{41}$$

Also on the basis of data by Bajura, we see that γ_2 increases with a decreasing ratio of riser to header flow

$$\theta_2 = 2\beta_2 - \gamma_2 \approx 2 - 0{\cdot}12(\tfrac{1}{60}N). \tag{42}$$

We must also estimate the turning-loss coefficients c_{TD} and c_{TC} occurring in equation (17). Based on data by Bajura (1971), $c_{TD} \approx 0{\cdot}4$, and depends only weakly on N. The data of McNown (1954) indicate that c_{TC} is also close to $0{\cdot}4$. Combining these estimates with that for K_3 (see Section 4), we see that

$$H_3 = M + f_3 L_3/D_3, \tag{43}$$

where $M \approx 4{\cdot}0$ is not strongly dependent on flow speed.

We cannot assume that the riser friction factor f_3 is independent of the flow speed $\bar{v}_3$. Good design practice (as we shall see below) is to have the riser diameter D_3 smaller than the header diameters D_1 and D_2, and to keep the pressure drop across each riser as small as that consistent with a good flow distribution. Well designed manifolds thus maintain laminar flow in the risers, so that

$$f_3 = 64/R_3 = 64\mu/\rho\bar{v}_3 D_3. \tag{44}$$

Using equation (10) we have

$$f_3 = -\frac{64\mu A_3}{\rho D_3 A_1}\frac{\mathrm{d}x_1}{\mathrm{d}\bar{v}_1}\frac{N_1}{L_1}, \tag{45}$$

so that

$$H_3 = M - \frac{64\mu L_3 A_3 N_1}{\rho D_3^2 A_1 \bar{v}_{1,0}}\frac{\mathrm{d}x}{\mathrm{d}v}. \tag{46}$$

Thus, in equation (28), dv/dx occurs on both the LHS and RHS. Defining

$$R_{1,0} = 64\mu/\rho\bar{v}_{1,0}D_1, \tag{47}$$

we solve (28) for dv/dx to obtain

$$\frac{dv}{dx} = [R_{1,0}(L_3 N_1/D_1) - \{R_{1,0}^2(L_3 N_1/D_1)^2 + 8A_r^2 M\Delta P\}^{\frac{1}{2}}]/2M. \tag{48}$$

Using equation (48), we can now write our pressure flow equations in the standard form suitable for numerical solution. Let the unknown functions be

$$y_1(x) = v(x), \qquad y_2(x) = \Delta P(x),$$

which then satisfy the pair of coupled nonlinear differential equations

$$y_1'(x) = F_1(y_2), \qquad y_2'(x) = F_2(y_1, y_2), \tag{49a, b}$$

where

$$F_1(y_2) = [R_{1,0}(L_3 N_1/D_1) - \{R_{1,0}^2(L_3 N_1/D_1)^2 + 8A_r^2 My_2\}^{\frac{1}{2}}]/2M, \tag{50}$$

$$F_2(y_1, y_2) = -A_1 y_1^2 + A_2(1-y_1)^2 + \{B_1 y_1 + B_2(1-y_1)\} \times A_r\left(\frac{2y_2}{M - R_{1,0}(L_3 N_1/D_1)\{1/F_1(y_2)\}}\right)^{\frac{1}{2}}. \tag{51}$$

Equations (49) must be solved subject to the boundary conditions

$$y_1(0) = 1, \qquad y_1(1) = 0. \tag{52}$$

The algorithm used to solve the boundary value problem (49) and (52) has been described by Haselgrove (1961).* It requires estimates to be provided for $y_2(0)$ and $y_2(1)$. The initial estimates for these are based on equal flow in all risers:

$$(\bar{v}_3)_{est} = \bar{v}_{1,0} D_1^2/ND_3^2, \tag{53}$$

$$y_2(0)|_{est} = y_1(0)|_{est} = \tfrac{1}{2}(M + f_3 L_3/D_3)(D_1^2/ND_3^2)^2. \tag{54}$$

If a preceding flow calculation has been made, the estimates (54) are corrected by the factors by which the estimates for the previous calculation were in error. Thus, if a whole series of similar calculations is being made, quite accurate initial estimates for $y_2(0)$ and $y_1(0)$ are generated.

The numerical solution of equations (49) and (52) proceeds iteratively. In all cases of reverse flow essayed the iteration converged, while for parallel flow it failed only in cases of highly non-uniform flow. The mechanism for the failure was that small errors in $P_1(x)$ and $P_2(x)$ when these quantities were approximately equal resulted in $P_1(x)$ falling below $P_2(x)$. When the flow pattern developed this unphysical feature, it was never able to converge.

* The algorithm is widely available in the package of scientific subroutines supplied by the Nottingham Algorithms Group in which it is called Algorithm DO2ADF.

Once the iteration converges, the values of $\bar{v}_1(x)$ and $\Delta\bar{P}_{12}(x)$ are known at a set of 20 or 30 mesh points x. The pressures $\bar{P}_1(x)$ and $\bar{P}_2(x)$ can be evaluated by quadrature:

$$\bar{P}_1 - \bar{P}_{1,0} = -\rho\bar{v}_{1,0}^2 \int_0^x \theta_1 F_1 v + \frac{f_1 L_1}{2D_1} v^2 \, dx, \tag{55}$$

$$\bar{P}_2 - \bar{P}_{2,0} = \rho v_{1,0}^2 \frac{D_1^4}{D_2^4} \int_0^x \theta_2 F_1 (1-v) - \frac{f_2 L_2}{2D_2}(1-v)^2 \, dx. \tag{56}$$

The expression (56) is for the case of parallel flow; for reverse flow, ρ should be replaced by $-\rho$, and $1-v$ by v. Note that equations (55) and (56) furnish an extra set of values of $\Delta\bar{P}_{12}(x)$, which can be used to check the set provided by the iterative solution of (49) and (52).

6. Comments on the Flow Model

In the development of the model, we used a momentum-balance argument to derive equations (8) and (14) for the variation of pressure along each header. An alternative approach would have been to use the Bernoulli equation for each header, neglecting transverse flow except in so far as it causes a change in header flow speed at each riser junction. The resulting formalism is a particular case of that used here, corresponding to the choices $\gamma_1 = \gamma_2 = 0$ and $\beta_1 = \beta_2 = 1$. It corresponds also to the use of conservation of energy rather than conservation of momentum in modelling flow near branch points (see Section 1). Note that the estimate used here for γ_1 is unity, while γ_2 differs significantly from zero only for a large number of risers.

We should point out that the values of the parameters θ_1, θ_2, c_{TD}, c_{TC} and K_3 used here are estimates, based on (sometimes inadequate) data on manifolds in the literature. However, our choices are justified by the good agreement obtained between theory and experiment. Note that the most appropriate values may well depend on the flow speed $\bar{v}_{1,0}$.

The flow model by Dunkle and Davey (1970) is also a particular case of the model used here. These authors took into account only frictional pressure losses, neglecting pressure changes associated through the Bernoulli equation with changes in fluid speed (i.e. $\theta_1 = \theta_2 = 0$ was used). They considered only parallel flow in a symmetric manifold ($L_1 = L_2$, $D_1 = D_2$), and assumed the flow to be turbulent in the headers ($f_1 = f_2 = f$ independent of flow rate) and laminar in the risers ($f_3 = 64/R_3$).

As we shall see in Section 7, in the manifold of Fig. 1 friction effects generally exceed Bernoulli effects on pressure, but the latter are by no means negligible in comparison. The flow model by Dunkle and Davey is then only a first-order approximation, giving flow patterns more uniform than those predicted by our more sophisticated model. Their model does, however, have the virtue that it can be solved analytically, without recourse to an iterative integration technique for solving a boundary value problem. Note that the computation times associated with both models are sufficiently low to permit economical real-time computer calculation of flow patterns.

As a final point, the flow model is a continuous one, with the number of risers N being important only in so far as it affects the total flow rate Q_T (equation 38) and the common header length L (equation 37). If L and Q_T are held constant, then variation of N has no effect on the computed flow patterns. Of course, in an actual manifold, this would not be the case, since the various flow parameters appropriate

at each riser junction would be affected by the conditions prevailing around all other riser junctions. Yet, for a fairly large number of risers (say N in excess of 10 or 15), we would expect the error inherent in using a continuous rather than a discrete model to be small.

7. Results for Collector Manifolds

We concentrate here on the manifold design given in Table 1. For each set of manifold conditions, we give two graphs, one showing the relative flow rate in the risers as a function of distance along the headers, the other showing the inlet and outlet header pressures as a function of distance. (Note that the quantity graphed as riser flow rate is actually that quantity multiplied by the number of risers. Thus, in a manifold with an entirely uniform flow distribution, the plotted quantity would be exactly equal to one at all values of x, irrespective of the number of risers.)

Figs 6–9 show the flow patterns in the manifold for between 15 and 60 risers, and for water temperatures varying between 30° and 120°C. The water temperature affects the flow distribution through its slight effect on density, but principally through its effect on viscosity. With increasing temperature, the viscosity decreases, and so the Reynolds number for a fixed fluid speed increases. Thus, the friction coefficient f_3 for the laminar flow in the risers decreases, leading to a lower pressure drop across the risers. The variation of pressure along the headers does not vary greatly with viscosity (since, although the pressure drop along the section of laminar flow decreases, turbulent flow begins earlier in the header, tending to increase the pressure drop along the remainder of the header). Increasing the water temperature thus decreases the pressure drop in the risers relative to that in the headers, and this results in less uniform flow.

We have just alluded to the most important principle concerning flow in manifolds: *if there is to be uniform flow, the pressure drop across the risers should significantly exceed the pressure drop across the headers.* This principle was discussed previously by Dunkle and Davey (1970). It is readily understood physically—think for example of the pressure curves of Fig. 9*b* representing voltages across a set of fixed resistors and the curves of Fig. 9*a* representing the corresponding currents. For low values of N, the principle is satisfied, the voltages being practically uniform, and the currents in their turn varying little. For high values of N, the pressure drops across risers and headers become comparable, so that voltages and currents vary markedly.

Note that the curves of flow rate are not symmetrical about $x = 0{\cdot}5$. In the model by Dunkle and Davey (1970), Bernoulli effects were ignored, the inlet and outlet headers were on an equal footing, and flow curves were always symmetrical. In our model, the inclusion of Bernoulli effects breaks the symmetry. We thus arrive at a second important principle, already enunciated by Bajura and Jones (1976): *in manifolds where Bernoulli effects on pressure are significant, the outlet header is more critical than the inlet header.* This also is readily understood physically: in the inlet header, flow is dropping off continually, leading to a Bernoulli regain of pressure opposing the frictional loss, whereas the increasing flow in the outlet header leads to a Bernoulli drop in pressure, reinforcing the frictional loss.

In the manifold of Fig. 1, frictional effects exceed pressure changes associated with the Bernoulli equation, but the latter are quite significant. Thus if different header diameters are contemplated, the diameter of the outlet header should exceed that of the inlet header. We will consider several asymmetric manifold designs below.

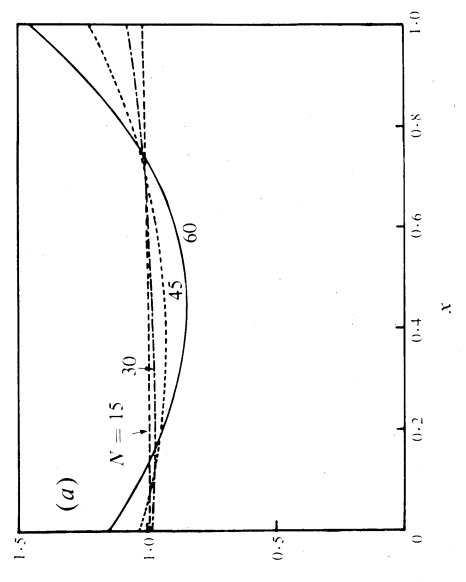

Fig. 6. Flow and pressure curves for the manifold of Table 1 ($T = 30°C$; $N = 60, 45, 30, 15$; parallel flow with a flow rate $Q_T = 1$ L min^{-1} per 15 risers): (*a*) variation of relative riser flow rate with distance x along manifold; (*b*) variation of pressure along the inlet (above) and outlet (below) headers with distance x.

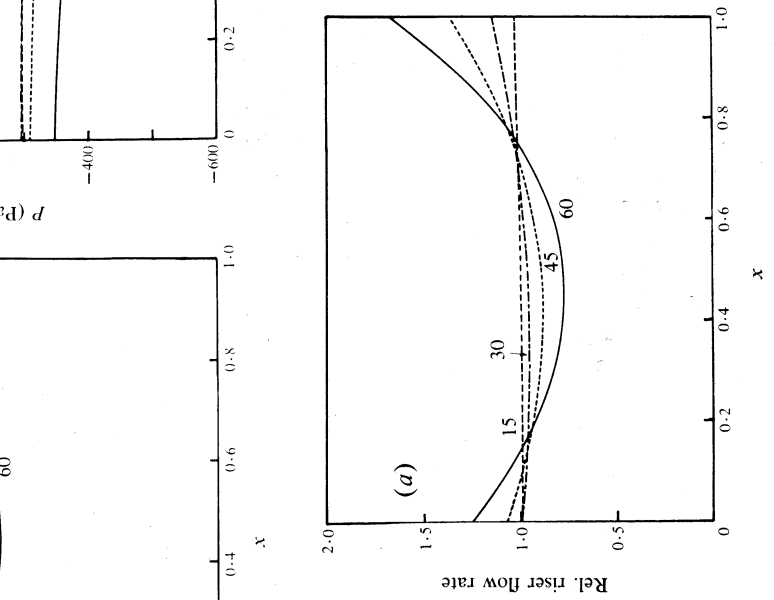

Fig. 7. As for Fig. 6, but with a water temperature of 60°C.

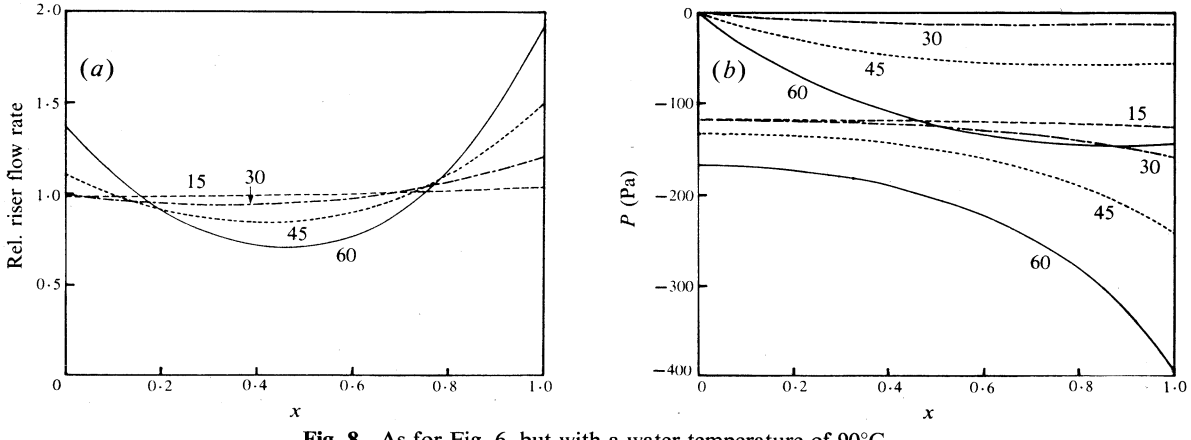

Fig. 8. As for Fig. 6, but with a water temperature of 90°C.

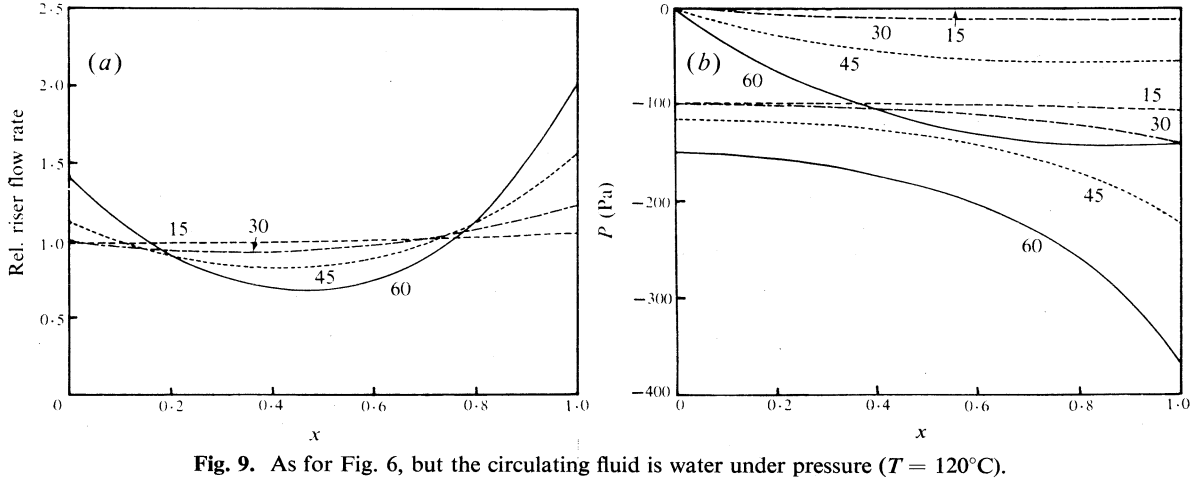

Fig. 9. As for Fig. 6, but the circulating fluid is water under pressure ($T = 120$°C).

Table 2. Flow ratio (FR) and head loss (HL, in Pa) for various temperatures

Results are for the manifold of Table 1, with parallel flow and a flow rate of 1 L min^{-1} per 15 risers

N	FR	HL	FR	HL
	30°C		60°C	
15	0·975	308	0·961	186
30	0·900	333	0·836	220
45	0·756	421	0·648	307
50	0·698	467	0·582	351
55	0·639	521	0·519	403
60	0·581	584	0·461	467
65	0·522	658	0·402	535
70	0·467	743	0·351	617
75	0·416	838		
	90°C		120°C	
15	0·943	125	0·936	107
30	0·775	159	0·753	140
45	0·558	244	0·527	222
50	0·490	286	0·456	263
55	0·425	336	0·392	312
60	0·366	394	0·334	367

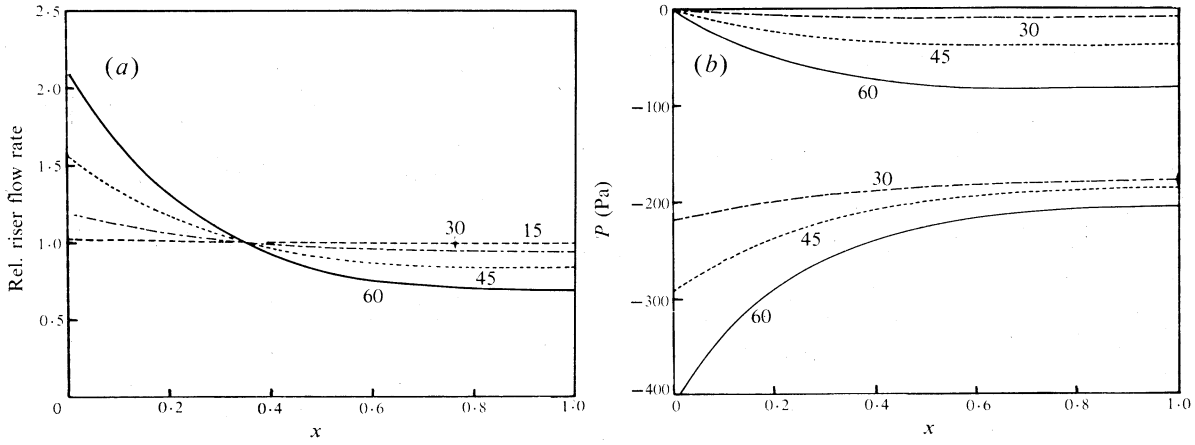

Fig. 10. As for Fig. 7, but with reverse flow in manifold.

Table 3. Comparison of reverse and parallel flow manifolds

N	FR	HL	FR	HL
	Reverse		Parallel	
15	0·966	186	0·961	186
30	0·789	219	0·836	220
45	0·531	293	0·648	307
60	0·327	410	0·461	467
65	0·277	457	0·402	535
70	0·235	508	0·351	617
75	0·200	561	0·301	703

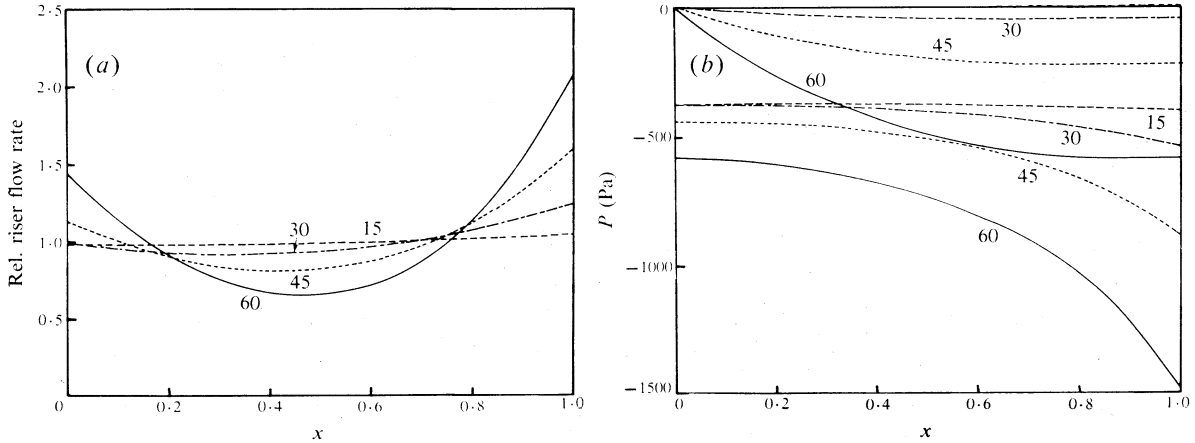

Fig. 11. As for Fig. 6, but $Q_T = 2\,\mathrm{L\,min^{-1}}$ per 15 risers.

Table 4. Comparison of performance of the manifold of Table 1 for two flow rates

N	FR	HL	FR	HL
	$1\,\mathrm{L\,min^{-1}}$		$2\,\mathrm{L\,min^{-1}}$	
15	0·961	186	0·930	408
30	0·836	220	0·737	547
45	0·648	307	0·506	889
50	0·582	351	0·436	1059
55	0·519	403	0·372	1258
60	0·461	467	0·313	1489

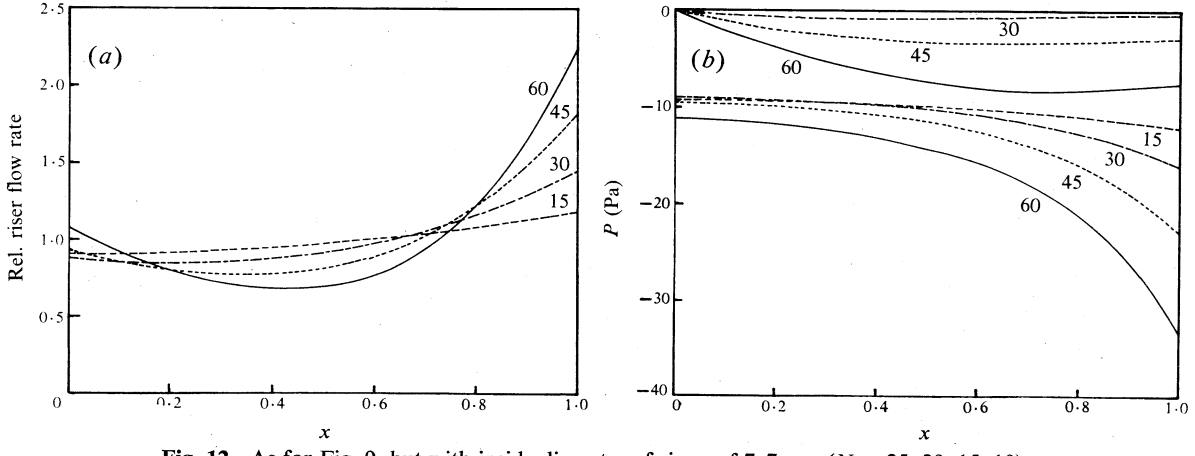

Fig. 12. As for Fig. 9, but with inside diameter of risers of 7·7 mm (N = 25, 20, 15, 10).

Table 5. Comparison of reverse and parallel flow manifolds

T = 120°C, internal diameters: headers 17·1 mm, risers 7·7 mm

N	FR	HL	FR	HL
	Reverse		Parallel	
5	0·958	11	0·930	11
10	0·827	12	0·762	12
15	0·602	15	0·580	16
20	0·398	21	0·428	23
25	0·257	29	0·303	34

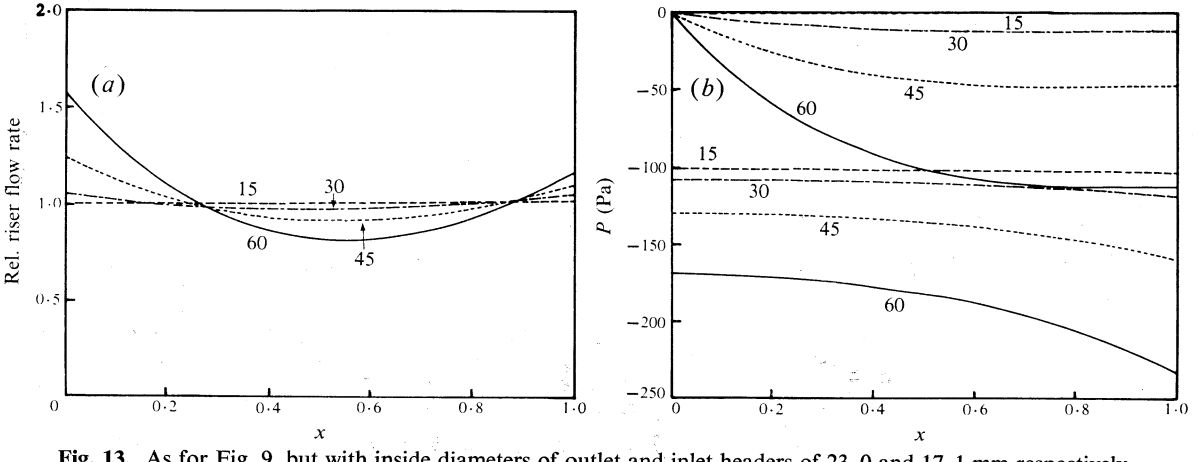

Fig. 13. As for Fig. 9, but with inside diameters of outlet and inlet headers of 23·0 and 17·1 mm respectively.

Table 6. Comparison of manifolds with 23·0 mm outlet headers and 4·4 mm risers, but with two different diameters of the inlet header

T = 120°C

N	FR	HL	FR	HL
	13·8 mm		17·1 mm	
15	0·978	104	0·979	103
30	0·772	137	0·921	118
45	0·477	217	0·733	159
50	0·399	254	0·659	180
55	0·334	296	0·585	205
60	—[A]	—[A]	0·516	233

[A] Calculation nonconvergent.

In Table 2, we summarize the performance of this manifold at the four temperatures 30°, 60°, 90° and 120°C. We give the flow ratio (the ratio of minimum to maximum riser flow rates) and the head loss (the total pressure drop across the manifold) as a function of the number of risers for each temperature. The minimum tolerable value for the flow ratio is a matter of judgment and will vary from case to case, but from Table 2 we see that (for the temperature range considered) 45–60 risers can be connected in parallel before the riser flow rates vary by about 2 : 1.

Thus far, we have considered only manifolds with parallel flow. In Fig. 10 we show curves corresponding to those in Fig. 7, but now for reverse rather than parallel flow. Except at the lowest flow rate ($N = 15$), flow uniformity is worsened by going from parallel to anti-parallel header streams. *The fact that frictional losses of pressure in the manifold exceed Bernoulli pressure changes means that parallel flow is preferable to reverse flow.*

The flow patterns in Fig. 10*a* are quite different from those in Fig. 7*a*. In Fig. 10*b* both inlet and outlet headers have their regions of most rapid pressure variation near $x = 0$, and so there is a monotonic decrease in riser flow rate as x increases. In Fig. 7*b*, the inlet pressure varies most rapidly near $x = 0$, where this header has maximum flow. The outlet pressure varies most rapidly near $x = 1$, again where the flow is maximal. Thus, there are two peaks in the riser flow rate, with the larger occurring at $x = 1{\cdot}0$ because of the predominance of the outlet header. The minimum riser flow rate thus occurs slightly below $x = 0{\cdot}5$. Note that the minimum flow rates in Fig. 7*a* tend to be slightly higher than their counterparts in Fig. 10*a*, while the maximum flow rates are lower in Fig. 7*a*. It is clearly desirable in these manifolds to have two separate regions of flow non-uniformity, rather than having the non-uniformities add up in one region.

We compare the reverse and parallel flow manifolds in Table 3. Note that head losses are lower for reverse flow than for the parallel flow geometry (so that pumping power requirements would be lower for reverse than for parallel flow). The reason for this difference in head loss is that, for the reverse flow arrangement, the flow in both headers decreases quite quickly as x increases from zero, leading to a shorter 'effective length' of the headers for frictional losses than in the parallel arrangement.

In assessing the importance of the head-loss advantage for the reverse flow configuration, it should be remembered that the actual head losses are quite small, and may be insignificant compared with head losses elsewhere in the collector system. Secondly, the worse flow patterns for this arrangement would result in a smaller number of risers capable of being placed in parallel, and thus a greater length of interconnecting pipes (with a greater head loss along them) for a given number of risers.

Bearing these points in mind, we limit the manifold studies below to the parallel flow arrangement. We complete our investigation of the manifold of Table 1 by illustrating its behaviour in Fig. 11 for a flow rate of 2 L min^{-1} rather than 1 L min^{-1}. As Table 4 shows, doubling the flow rate more than doubles the head loss, but it decreases the number of risers at which a given flow ratio occurs by around 20% in the critical region (where flow ratios are around 0·5).

Consider the effect of increasing the riser internal diameter from 4·4 to 7·7 mm. In Fig. 12 we illustrate the resulting flow patterns for the parallel configuration (with a water temperature of 120°C). In Table 5, we compare the performance of the parallel and reverse arrangements. It will be noticed that the flow ratios for the two arrangements are much closer here than in Table 3, as a consequence of Bernoulli effects now

being larger in comparison with frictional head losses. Comparing Tables 2 and 5, we see that the increase in riser diameter has had a dramatic effect in worsening flow patterns: as a corollary to the most important principle of design enunciated above, *the ratio of riser diameter to header diameter is the most important choice in the design of a collector manifold.* The numbers of risers for corresponding flow ratios have decreased by the riser diameter ratio to a power of about 1·6 in going from Table 2 to Table 5.

Let us now consider the behaviour of manifolds in which the diameter of the outlet header exceeds that of the inlet header. In Fig. 13 we show the flow patterns for a manifold having an outlet diameter of 23·0 mm, and an inlet diameter of 17·1 mm. It will be noticed that pressure changes in the inlet header now exceed those in the outlet header (the opposite ordering having prevailed in all other manifolds considered above). In Table 6 we compare the behaviour of the manifold with one having the inlet header diameter reduced to 13·8 mm. The flow patterns are significantly worse, since we have increased the ratio of inlet to outlet header pressure drops even further. We suggest that *an optimal manifold design would have the inlet and outlet header diameters chosen to equalize their pressure drops.*

8. Comparison with Experiment

An array of evacuated collectors with dimensions as given in Table 1 was constructed in order to provide data for comparison with the preceding analysis. For convenience, 15 risers were grouped together into panels. The panels were connected together with short lengths of flexible hose of 20 mm internal diameter, the risers in adjacent panels being separated by 160 mm. Each riser was enclosed by an all-glass evacuated solar collector tube and connected to it thermally by a heat transfer fin (Fig. 1). The tubes were very similar in characteristics, so that the same heat input was made into each riser.

Flow rate in the risers was not measured directly, but deduced by measurement of the temperature rise. An inverse relation between flow rate and temperature rise will hold provided that the temperature rise is sufficiently small so that isothermal flow is still a good approximation. As the quantity we are interested in is the flow ratio (FR) and not the absolute value of flow, the precise relation between temperature rise and flow rate is not required. This measurement procedure is not only more convenient than a direct measurement of the flow rate but avoids perturbations to flow due to the introduction of any measurement impedance.

The temperature rise was measured by a set of copper–constantan thermocouples wired as differential pairs, with constantan being used as the intermediate metal. Every third riser was monitored and the thermocouples were scanned by a digital data logger so that plots of riser number against temperature rise could be obtained in a few seconds at any desired time. The zero levels of the thermocouples were adjusted to give consistent readings. Measurements were made with parallel flow for riser numbers of 30, 45 and 60, and temperatures of 20°, 30° and 60°C, with flow rates of 1 and 2 $L\,min^{-1}$ for each panel of 15 risers. One measurement was made with reverse flow at 20°C for the case of 60 risers and 1 $L\,min^{-1}$ flow rate.

Comparison of the experimental variation of flow rate with position in the array is made in Fig. 14 for parallel flow. The agreement between theory and experiment is excellent. In particular, the asymmetry of flow about the centre of the array is quite evident in the experimental points. A slight deviation of the last experimental measurement may indicate an end effect which is not included in the theory.

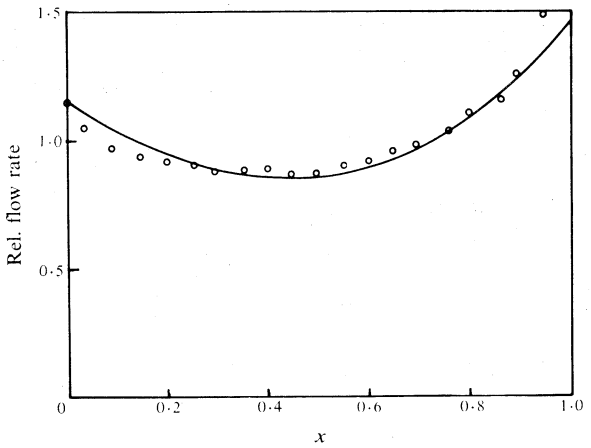

Fig. 14. Relative flow rate in risers of the manifold of Table 1 with parallel flow, as a function of distance along the manifold. The points are experimental and the curve is the corresponding theoretical prediction.

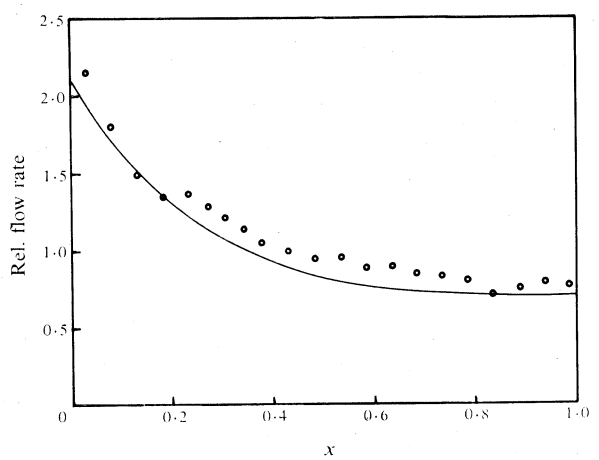

Fig. 15. As for Fig. 14, but with reverse flow.

Table 7. Comparison of calculated and measured flow ratios at various temperatures, flow rates Q per 15 risers and number of risers N

N	20°C $Q = 2\,\mathrm{L\,min^{-1}}$		30°C $Q = 1\,\mathrm{L\,min^{-1}}$		60°C $Q = 1\,\mathrm{L\,min^{-1}}$		60°C $Q = 2\,\mathrm{L\,min^{-1}}$	
	Expt	Theory	Expt	Theory	Expt	Theory	Expt	Theory
30	0·85	0·84	0·89	0·90	0·87	0·84	0·70	0·74
45	0·73	0·66	0·76	0·76	0·65	0·65	0·50	0·51
60	0·53	0·47	0·59	0·58	0·47	0·46	0·30	0·31

The corresponding comparison for reverse flow is made in Fig. 15. The agreement is again excellent, the only significant deviation being the first measured point, which may be subject to an end effect. The superiority of the parallel flow over the reverse flow configuration is evident by a comparison of the experimental results of Figs 14 and 15.

In Table 7 we compare the theoretical predictions with experimental measurements of the flow rate for the manifold of Table 1. The accuracy of the experimental values is estimated to be $\pm 0{\cdot}02$. The agreement between theory and experiment is on the whole excellent. All the theoretical predictions concerning the variation of flow ratio with temperature, number of risers and flow rate are confirmed by the measurements.

9. Effect of Temperature on Flow Distribution

The theoretical model described above is an isothermal one. It is possible to estimate the pressure differences across risers associated with heating of the fluid in them, in order to compare them with the isothermal pressure differences. For a U-shaped riser tube with arms of length l inclined at an angle ϕ to the horizontal, the pressure difference due to a density difference in the arms is

$$\Delta P = gl \sin \phi (\rho_1 - \rho_2), \tag{57}$$

where ρ_1 and ρ_2 are the average densities in each arm. Taking a typical case in which $l = 1{\cdot}45$ m, $\phi = 34°$ and the temperature rise across the riser is 20°C, we find ΔP to be 16 Pa.

The pressure differences in Figs 6–13 are around 150 Pa or greater. Thus the head due to density differences (thermosiphon effects) does not play a major part in determining the flow distributions we have considered above.

Let us now discuss a manifold for which the risers are larger than the headers. We have considered numerically a manifold with the risers of internal diameter $13{\cdot}3$ mm and the headers of diameter $12{\cdot}0$ mm. With a flow rate of $1{\cdot}25$ L min^{-1} per 15 risers, the flow ratio decreased very rapidly with increasing number of risers, having the value $0{\cdot}15$ for $N = 10$. With the large riser diameter the pressure differences between headers were small, for example $2{\cdot}9$ Pa for $N = 10$. For this manifold then, the thermosiphon effects are most important.

Such a manifold has been constructed and its flow distributions studied qualitatively at various flow rates. At a flow rate of $1{\cdot}25$ L min^{-1} per 15 risers and $N = 20$, flow was observed to be very fast in the outer risers of the array and very slow in the middle third of the array. On increasing the flow rate to $2{\cdot}25$ L min^{-1} the flow in the central regions deteriorated and, in fact, flow reversal was observed in one riser (number 13 from the inlet). The thermosiphon effect was present in this experiment as the risers were contained in evacuated tubular collectors exposed to solar flux, but clearly this cannot be the mechanism for the onset of counter flow with increasing flow rate.

The occurrence of counter flow in manifolds has been noted previously. Bajura and Jones (1976) stated that this flow reversal may occur near the inlet of a manifold, due to the presence of out-of-plane bends in the inlet pipework. Such bends give rise to velocity profiles which depend on x for small x, so that allowance must be made for nonzero $\mathrm{d}\beta/\mathrm{d}x$ in equations (32). Bajura and Jones stated that this momentum correction term in (32) is the only mechanism by which the flow reversal phenomenon can be explained analytically. However, this correction term is expected to be zero in the central region of the manifold in which we observed reversal of flow.

Note that a local change in the area of either header pipe near a riser would affect the pressure drop across that riser. The fractional change in area of a header which corresponds to a change in pressure of 2·9 Pa with a flow rate of 2·25 L min^{-1} is 6%. Area changes larger than this would cause reversal of flow in the manifold. We consider this to be the explanation of our observations.

Window and Harding (1982) have discussed the effect of density changes on flow in a solar collector manifold containing a small number of risers. Thermosiphon effects were found to improve the flow uniformity, as would be expected. Their measurements showed that, in the isothermal case where the manifold was practically horizontal, the flow patterns were qualitatively similar to those we have calculated for manifolds in which Bernoulli pressure changes exceed those due to friction.

Although thermosiphon effects can help to balance the flow in manifolds in which reversal of flow does not occur, it cannot be relied on to overcome reverse flow when it does occur. Once reverse flow has been established in a riser, thermosiphon effects will reinforce rather than counter the trend. Experiments carried out on a single upright U tube inclined at 34° to the horizontal and inserted into an evacuated tubular collector (Fig. 1) showed that thermosiphon flow could indeed be established in either direction. Thus, in order to obtain a manifold in which reversal of flow will never occur, with or without thermosiphon effects present, a good isothermal flow pattern is necessary.

10. Conclusions

We have developed a model for isothermal flow in parallel connected solar collector manifolds based on the work of Bajura and Jones (1976). The predicted flow patterns are in excellent agreement with experimental results. This good agreement justifies the use of a continuous model and verifies our estimates of the critical flow parameters.

The implications of the model for the design of such manifolds have been examined. Among the main conclusions are the importance of the ratio of riser to header diameter and the potential advantages to be gained from a manifold in which the outlet header diameter exceeds that of the inlet header. We note that well designed manifolds permit satisfactory flow uniformity with at least 60 risers in parallel. An equally important conclusion is the superior flow uniformity obtainable with parallel as opposed to reverse flow streams in the header pipes.

Thermosiphon effects become important in manifolds with large non-uniformity of flow and when pressure drops across risers are of the order of 16 Pa in the manifolds considered. Under these conditions reversal of flow in risers can easily occur due to imperfections in the manifold construction.

Acknowledgments

The authors acknowledge the experimental assistance of M. R. Riley and I. C. Onley, valuable discussions with Dr A. Lozzi and the encouragement of Professor H. Messel. The financial support of the Government of New South Wales and His Royal Highness Prince Nawaf Bin Abdul Aziz of the Kingdom of Saudi Arabia through the Science Foundation for Physics is gratefully acknowledged.

References

Bajura, R. A. (1971). *Trans. ASME* **93**, 7–12.
Bajura, R. A., and Jones, E. K. (1976). *Trans. ASME* **98**, 654–65.

Dunkle, R. V., and Davey, E. T. (1970). Proc. I.S.E.S. Conf., Melbourne (I.S.E.S.: Melbourne).
Hansen, A. G. (1967). 'Fluid Mechanics', p. 420 (Wiley and Sons: New York).
Haselgrove, C. B. (1961). *Comput. J.* **4**, 255–9.
Jones, G. F., and Lior, N. (1978). Proc. I.S.E.S. Conf., Denver (I.S.E.S.: America).
Kenyon, R. A. (1960). 'Principles of Fluid Mechanics', pp. 165–9 (Ronald: New York).
McNown, J. S. (1954). *Trans. ASCE* **119**, 1103–18.
Swanson, W. M. (1970). 'Fluid Mechanics', p. 431 (Holt, Rinehart and Winston: New York).
Window, B., and Harding, G. L. (1983). *Sol. Energy* (submitted).

Manuscript received 6 August, accepted 8 November 1982